AGU PUBLICATIONS

JGR

Journal of Geophysical Research: Space Physics

RESEARCH ARTICLE
10.1002/2015JA021637

Key Points:
- Using Joule heating rate as the neutral-ion energy coupling led to a cooler thermosphere
- Neutral photoelectron heating efficiency compensates for the missing heating
- A slight dependence of the underestimation of T_n on $F_{10.7}$ existed

Correspondence to:
J. Zhu,
zhjie@umich.edu

Citation:
Zhu, J., and A. J. Ridley (2016), Investigating the performance of simplified neutral-ion collisional heating rate in a global IT model, *J. Geophys. Res. Space Physics*, *121*, 578–588, doi:10.1002/2015JA021637.

Received 30 JUN 2015
Accepted 9 DEC 2015
Accepted article online 15 DEC 2015
Published online 11 JAN 2016

Investigating the performance of simplified neutral-ion collisional heating rate in a global IT model

Jie Zhu[1] and Aaron J. Ridley[1]

[1]Department of Atmospheric, Oceanic and Space Sciences, University of Michigan, Ann Arbor, Michigan, USA

Abstract The Joule heating rate has usually been used as an approximate form of the neutral-ion collisional heating rate in the thermospheric energy equation in global thermosphere-ionosphere models. This means that the energy coupling has ignored the energy gained by the ions from collisions with electrons. It was found that the globally averaged thermospheric temperature (T_n) was underestimated in simulations using the Joule heating rate, by about 11% when $F_{10.7} = 110$ solar flux unit (sfu, 1 sfu = 10^{-22} W m^{-2} Hz^{-1}) in a quiet geomagnetic condition. The underestimation of T_n was higher at low latitudes than high latitudes, and higher at *F* region altitudes than at *E* region altitudes. It was found that adding additional neutral photoelectron heating in a global IT model compensated for the underestimation of T_n using the Joule heating approximation. Adding direct photoelectron heating to the neutrals compensated for the indirect path for the energy that flows from the electrons to the ions then to the neutrals naturally and therefore was an adequate compensation over the dayside. There was a slight dependence of the underestimation of T_n on $F_{10.7}$, such that larger activity levels resulted in a need for more compensation in direct photoelectron heating to the neutrals to make up for the neglected indirect heating through ions and electrons.

1. Introduction

The energy coupling between the ionospheric plasma and the neutral atmosphere strongly affects the global energy budget and temperature distribution of the thermosphere. Ionosphere-thermosphere models usually use the Joule heating approximation as the neutral-ion energy coupling term in the neutral energy equation [*Roble et al.*, 1988; *Fuller-Rowell and Rees*, 1980; *Zhu et al.*, 2005]. Various studies have shown that Joule heating [*Cole*, 1962, 1971] is one of the major energy sources of the upper atmosphere at high latitudes using satellite [*Heelis and Coley*, 1988; *Gary et al.*, 1995; *Liu and Lühr*, 2005] and ground-based measurements [*Banks et al.*, 1981; *Thayer*, 1998], as well as using coupled global ionosphere-thermosphere models [*Barth et al.*, 2009; *Fuller-Rowell et al.*, 1996; *Rodger et al.*, 2001; *Deng et al.*, 2011]. *Codrescu et al.* [1995] suggested that Joule heating could be significantly underestimated by the exclusion of small-scale variability of *E* field in high-latitude convection models. *Deng and Ridley* [2007] further pointed out that model resolution and the vertical differences between ion and neutral velocity were other two sources for an underestimation of Joule heating within global IT models. *Emery et al.* [1999] suggested that a corrective multiplicative factor of 2.5 of the Joule heating rate was needed for the winter hemisphere in order to account for small-scale structures and rapid variability in high-latitude electric fields. Significant efforts have been made to quantify various uncertainties existing in modeling the Joule heating rate. However, despite the widespread use of the Joule heating rate as an approximation of the neutral-ion collisional heating rate in the neutral energy equation, there have been few studies showing how well the Joule heating rate performs in a global ionosphere-thermosphere model.

Solar radiation in Extreme Ultraviolet (EUV) and soft X-ray wavelengths is the dominant energy source of the upper atmosphere. It is known that the solar radiation energy primarily goes directly into photoionization and molecular dissociation [*Torr et al.*, 1980]. Photoelectrons are produced through the photoionization process, carrying photon energy in excess of the ionization threshold as kinetic energy. Photoelectrons are then responsible for heating the ambient thermal electrons [*Smithtro and Solomon*, 2008]. Efforts have been made to develop a physical model to solve photoelectron flux and energy spectra considering transport, elastic and inelastic collisions, and energy loss to ambient electrons [*Nagy and Banks*, 1970; *Richards and Torr*, 1983; *Torr et al.*, 1990]. A parameterization of the electron volume heating rate by photoelectrons was developed by *Swartz and Nisbet* [1972]. An improved parameterization was further developed for application to

photoelectron heating of ambient thermal electrons during solar flares [*Smithtro and Solomon*, 2008]. It was suggested that neutrals were indirectly heated by photoelectrons: collisions between photoelectrons and thermal electrons produced hot electrons which heat neutrals and ions through elastic and inelastic collisions [*Torr et al.*, 1980; *Roble and Emery*, 1983; *Aggarwal et al.*, 1979]. The electron-ion collisions dominate over the electron-neutral collisions above the *E* region [*Aggarwal et al.*, 1979]. A constant photoelectron heating efficiency of ~0.05 has been applied in global ionosphere-thermosphere models such as the Thermosphere Ionosphere Electrodynamics General Circulation Model [*Roble et al.*, 1988; *Richmond*, 1995] and the Global Ionosphere-Thermosphere Model (GITM) [*Ridley et al.*, 2006] in order to compensate for the discrepancy in the thermospheric temperature between model results and observations [*Burrell et al.*, 2015; *Maute*, 2011]. However, there have been few literatures investigating whether there exists direct photoelectron heating to the neutral atmosphere or quantifying the neutral photoelectron heating efficiency for the neutral atmosphere either by observation or by numerical calculation to the author's knowledge.

In this study, through the investigation of the performance of the Joule heating rate as an approximate form of the neutral-ion energy coupling rate in GITM, an explanation (or a justification) for using a photoelectron heating efficiency for the neutral atmosphere will be presented. To fully consider the neutral-ion energy coupling, a complete neutral-ion collisional heating terms need to be considered. Two forms of the neutral-ion heating rate were implemented in GITM: the simplified Joule heating rate and a more complete energy equation that allows energy flow from the electrons to the ions then to the neutrals. The influence of the two forms of neutral-ion heating rate on the thermospheric temperature was investigated and three questions will be explored: (a) How much has T_n been underestimated or overestimated by using the Joule heating as the neutral-ion energy coupling term? (b) How did the performance of the Joule heating term change with altitude, latitude, and local time? (c) How accurately has the neutral photoelectron heating used in global IT models compensated for the missing heating?

2. Methodology

The Global Ionosphere-Thermosphere Model is a three-dimensional model that couples the ionosphere-thermosphere system in spherical coordinates [*Ridley et al.*, 2006]. In this study, the *Weimer* [2005] model was used for the high-latitude electric fields, and the *Fuller-Rowell and Evans* [1987] model was employed to produce the auroral precipitation pattern. A dynamo electric field was solved for in a self-consistent way by using the techniques described in *Richmond* [1995] and *Vichare et al.* [2012]. This study used the recently updated GITM, in which the neutral, ion, and electron energies are fully coupled (J. Zhu and A. J. Ridley, Simulating electron and ion temperature in a global ionosphere-thermosphere model: Validation and modeling an idealized substorm, submitted to *Journal of Atmospheric and Solar-Terrestrial Physics*, 2015).

The complete neutral-ion collisional heating rate can be written as [*Banks and Kockarts*, 1973; *Schunk*, 1975]:

$$Q_C = \sum_k n_k m_k \sum_t \frac{\nu_{kt}}{m_k + m_t} \left[3\kappa(T_i - T_n) + m_t(\boldsymbol{u_n} - \boldsymbol{u_i})^2\right], \tag{1}$$

where n, m, and T are the number density, mass, and temperature respectively, $\boldsymbol{u_n}$ and $\boldsymbol{u_i}$ are the neutral and ion velocities, and the subscripts t and k denote the ion and neutral species, respectively, while the subscripts i and n denote the bulk ion and neutrals, respectively. Specifically, the term "neutral-ion" was used for source terms in the neutral energy equation and the term "ion-neutral" was used in the ion energy equation here. The first term is the heat transfer rate from the ions to the neutrals, with the second term being the neutral-ion frictional heating rate due to the velocity difference between the two species [*Banks and Kockarts*, 1973; *Schunk*, 1975].

Generally, the ion temperature can be assumed to be in steady state and balanced by energy coupling to both neutrals and electrons:

$$3\kappa(T_i - T_n) = m_n(\boldsymbol{u_n} - \boldsymbol{u_i})^2 + \frac{m_i + m_n}{m_i}\frac{\nu_{ie}}{\nu_{in}}(3\kappa(T_e - T_i) + m_e(\boldsymbol{u_e} - \boldsymbol{u_i})^2), \tag{2}$$

where ν_{ie} and ν_{in} are the collisional frequencies between ions and electrons and between ions and neutrals, respectively. Considering $m_e \ll m_i$, the ion-electron frictional heating rate can be ignored, and equation (2) can be simplified to

$$3\kappa(T_i - T_n) = m_n(\boldsymbol{u_n} - \boldsymbol{u_i})^2 + \frac{m_i + m_n}{m_i}\frac{\nu_{ie}}{\nu_{in}}3\kappa(T_e - T_i). \tag{3}$$

At high latitudes or on the nightside when the electron density is low, ν_{ie} can be much less than ν_{in}. Thus, a balance can be approximated between the ion-neutral heat transfer rate and the ion-neutral frictional heating rate, and the ion energy equation can be simplified to

$$3\kappa(T_i - T_n) \cong m_n(\boldsymbol{u_n} - \boldsymbol{u_i})^2. \tag{4}$$

This assumption has been widely applied for large temporal and spatial ionospheric structure at high latitudes when the ion density is low [*St-Maurice and Hanson*, 1982; *Killeen et al.*, 1984; *Schunk and Nagy*, 2009; *Thayer and Semeter*, 2004].

This approximation can be substituted into equation (1), so that the complete neutral-ion collisional heating rate can be written as

$$Q_C \approx Q_J = \sum_k n_k m_k \sum_t \frac{\nu_{kt}}{m_k + m_t}\left[m_k(\boldsymbol{u_n} - \boldsymbol{u_i})^2 + m_t(\boldsymbol{u_n} - \boldsymbol{u_i})^2\right]. \tag{5}$$

This is consistent with the suggestion by *St-Maurice and Hanson* [1982] that the Joule heating rate was twice the neutral-ion frictional heating assuming $m_k \approx m_t$. This equivalence was confirmed by in situ measurements by the Atmosphere Explorer satellites around the 1980s [*St-Maurice and Hanson*, 1982].

Using the relation

$$n_n m_n \nu_{ni} = n_i m_i \nu_{in}, \tag{6}$$

the neutral-ion collisional heating rate in equation (5) can be written as

$$Q_J = \sum_t n_t m_t \sum_k \nu_{tk}(\boldsymbol{u_n} - \boldsymbol{u_i})^2. \tag{7}$$

If the ion and electron motion perpendicular to the magnetic field is in steady state and determined only by the Lorentz and ion drag force, the electron gyrofrequency is much greater than the electron-neutral collisional frequency which is true above 90 km [*Brekke*, 2012; *Thayer and Semeter*, 2004; *Strangeway*, 2012], Q_J is equivalent to the Joule heating rate

$$Q_J = \boldsymbol{j} \cdot \boldsymbol{E}'. \tag{8}$$

Here $\boldsymbol{j}$ is current and $\boldsymbol{E}'$ is the electric field in the neutral gas frame [*Thayer and Semeter*, 2004].

The errors in the temporal change rate of T_n using Joule heating rate can be estimated by subtracting the time rate of change of T_n due to Q_J from that due to Q_C. The time rate of change of the neutral temperature due to the neutral-ion energy coupling is given by

$$\frac{\mathrm{d}T_n}{\mathrm{d}t} = \frac{Q}{\kappa \sum_k n_k m_k}, \tag{9}$$

where κ is the Boltzmann constant, and Q stands for either the complete neutral-ion collisional heating rate as shown in equation (1) or the Joule heating rate as shown in equation (7). For simplicity, the mean mass (i.e., number density weighted mass) was applied for the neutrals ($\bar{m}_n$) and ions ($\bar{m}_i$) in the following calculation. In order to explain the errors in the simplification in going from the more complete equation to the Joule heating simplification, the difference between the two can be explored and expressed as

$$\Delta\frac{\mathrm{d}T_n}{\mathrm{d}t} \propto \frac{Q_C - Q_J}{n_n \bar{m}_n \kappa}. \tag{10}$$

Q_C in equation (1) was simplified to

$$Q_{C_s} = n_n \bar{m}_n \frac{\nu_{ni}}{\bar{m}_n + \bar{m}_i}\left[3\kappa(T_i - T_n) + \bar{m}_i(\boldsymbol{u_n} - \boldsymbol{u_i})^2\right], \tag{11}$$

while Q_J in equation (5) was simplified to

$$Q_{J_s} = n_n \bar{m}_n \frac{\nu_{ni}}{\bar{m}_n + \bar{m}_i} \left[\bar{m}_n (\boldsymbol{u_n} - \boldsymbol{u_i})^2 + \bar{m}_i (\boldsymbol{u_n} - \boldsymbol{u_i})^2 \right]. \tag{12}$$

Substituting Q_{C_s} and Q_{J_s} into equation (10) leads to

$$\Delta \frac{\mathrm{d}T_n}{\mathrm{d}t} \propto \frac{\nu_{ni}}{\kappa(\bar{m}_n + \bar{m}_i)} \left[3\kappa(T_i - T_n) - \bar{m}_n (\boldsymbol{u_n} - \boldsymbol{u_i})^2 \right]. \tag{13}$$

Substituting equation (3) into equation (13) and assuming $\bar{m}_n \approx \bar{m}_i$ result in

$$\Delta \frac{\mathrm{d}T_n}{\mathrm{d}t} \propto \frac{\nu_{ie}}{\bar{m}_i} 3(T_e - T_i). \tag{14}$$

Considering the electron-ion collision frequency in s^{-1} [*Schunk and Nagy*, 2009]

$$\nu_{ei} = 5.44 \times 10^{-5} \frac{n_i Z_i^2}{T_e^{3/2}}, \tag{15}$$

where n_i is the ion number density in m^{-3}, Z_i is the number of ion charge, T_e is in K and 54.4 is in $\mathrm{s}^{-1}\ \mathrm{K}^{\frac{3}{2}}\ \mathrm{m}^3$, and the relation

$$n_e m_e \nu_{ei} = n_i m_i \nu_{ie} \tag{16}$$

is used. Equation (14) can be further expressed as

$$\Delta \frac{\mathrm{d}T_n}{\mathrm{d}t} \propto \left(3\kappa \frac{5.44 \times 10^{-5} Z_i^2 m_e}{\bar{m}_i^2} \right) \frac{n_i}{T_e^{\frac{3}{2}}} (T_e - T_i) \propto \frac{n_i}{T_e^{\frac{3}{2}}} (T_e - T_i). \tag{17}$$

Here the variation of the neutral-ion collisional frequency (which is neutral density dependent) was ignored. This equation shows that the Joule heating approximation is valid in regions in which either (a) the ion density is quite low or (b) the temperature difference between the ions and electrons is small. As noted by *St-Maurice and Hanson* [1982], *Killeen et al.* [1984], *Schunk and Nagy* [2009], and *Thayer and Semeter* [2004], these conditions tend to occur at high latitudes.

The heating rates are defined for reference below. The ion-neutral frictional heating rate is

$$Q_F(I-N) = \sum_t n_t m_t \sum_k \frac{m_k \nu_{tk}}{m_t + m_k} (\boldsymbol{u_n} - \boldsymbol{u_i})^2, \tag{18}$$

and the ion-neutral heat transfer rate is

$$Q_T(I-N) = \sum_t n_t m_t \sum_k \frac{3\kappa \nu_{tk}}{m_t + m_k} (T_i - T_n). \tag{19}$$

The ion-electron heat transfer rate is expressed as

$$Q_T(I-E) = \sum_t n_t m_t \frac{3\kappa \nu_{te}}{m_t + m_e} (T_i - T_e). \tag{20}$$

In this study, the complete neutral-ion collisional heating rate in equation (1) and the Joule heating rate in equation (7) were implemented in the Global Ionosphere-Thermosphere Model. First, a set of simulations were conducted during the winter solstice, i.e., 21–23 December 2012. The first simulation used a complete neutral-ion collisional heating rate with zero photoelectron heating efficiency (PHE) (termed the Complete simulation). The second simulation used the Joule heating rate as an approximate form of the neutral-ion collisional heating rate with zero PHE (termed the Joule simulation). The third simulation (termed the Joule simulation with 0.05 PHE) is the same as the Joule simulation except with a PHE efficiency of 0.05. All external drivers in the three simulations were the same and constant: the $F_{10.7}$ index was 110 sfu (sfu, 1 sfu = $10^{-22}\ \mathrm{W\ m^{-2}\ Hz^{-1}}$), interplanetary magnetic field (IMF) B_z was southward with the value of −2 nT and the IMF B_y was 0 nT, the solar wind speed was 400 km/s, and the hemispheric power was set to 20 GW. The dynamo solver was turned on in all the simulations. The grid size was 2.5° longitude by 1.0° latitude. The altitudinal grid size was stretched to about one third of a scale height based on the initial thermospheric temperature and density. Also, the same set of simulations were conducted with two different $F_{10.7}$: 70 sfu and 150 sfu,

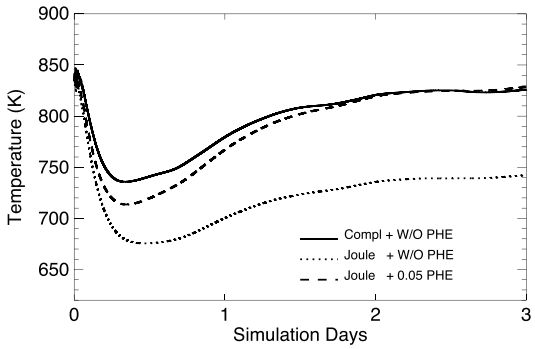

Figure 1. The evolution of the global averaged neutral temperature over three simulation days beginning from 00 UT 24 December 2012. The solid line shows the simulation using the complete neutral-ion collisional heating rate with PHE equal to zero (termed as the Complete simulation). The dotted line shows the simulation using the Joule heating rate with PHE equal to zero (termed as the Joule simulation). The dashed line shows the simulation using the Joule heating rate with PHE equal to 0.05 (termed as the Joule simulation with 0.05 PHE).

in order to explore the dependence of the Joule heating approximation on solar irradiance and justify the photoelectron heating efficiency used to compensate the missing heating.

3. Results

3.1. Comparison Between the Complete and Joule Simulations

Figure 1 shows the temporal variation of the globally volume-averaged neutral temperature over three simulation days for the three cases. The globally averaged temperature was plotted to illustrate the evolution of the simulations into a steady state. In all three cases, the globally averaged T_n decreased quickly during the first 5 h, increased gradually, and leveled off at the beginning of the third day. T_n dropped in the beginning of the simulation because GITM does not assume a hydrostatic solution [*Ridley et al.*, 2006], and it is initialized with Mass Spectrometer Incoherent Scatter [*Hedin et al.*, 1977], which does not have a perfectly hydrostatic balance. There were massive modifications of the dynamics that took place over the beginning of the simulations. T_n in the Joule simulation leveled off at around 740 K, which was about 90 K (~11%) lower than the Complete simulation. This was expected because the Joule heating rate did not account for the ion-electron heat transfer in the ion thermal equation. This resulted in an underestimation of $T_i - T_n$ as shown in equation (4), thus leading to a lower neutral-ion heat transfer rate for the neutrals. This phenomenon tends to occur in the dayside *F* region where the ion densities are large and the electron temperature becomes progressively larger than the ion temperature [*Roble*, 1975]. The third simulation, which is the normal method in global IT models, used the Joule heating rate with a nonzero neutral photoelectron heating efficiency. Different PHE values were tested (not shown here), and it was found that a Joule simulation with PHE equal to 0.05 had approximately the same globally averaged T_n as the Complete simulation, as shown by the dashed line in Figure 1.

Figure 2 shows the comparison of the T_n distribution between the three simulations. Figure 2 (top row) shows the global horizontal distribution at 300 km of T_n for the three cases. The Joule simulation (i.e., Figure 2, middle column) shows a similar distribution of the neutral temperature as the Complete simulation (i.e., Figure 2, left column); however, a difference of about 100 K existed globally at 300 km between the Complete and Joule simulations. Although it was expected that it would be the dayside where the Joule heating rate most deviated from the complete neutral-ion collisional heating rate, there was also about 100 K difference in the nightside *F* region. This was due to neutral winds advecting the increased temperature from the dayside to the nightside. The comparison of T_n at 180° longitude (middle row) and at 300 km altitude above 50° latitude (bottom row) were shown in Figure 2. Large temperature differences are observed in these cuts as well. By increasing the photoelectron heating efficiency to 0.05, the Joule simulation with 0.05 PHE, as shown in Figure 2 (right column), showed a similar global distribution as the Complete simulation excluding photoelectron heating for the neutrals.

The compensation for the underestimation of T_n in the Joule simulation by the neutral photoelectron heating efficiency was not a coincidence. The approximation of the neutral-ion energy coupling by the Joule heating rate is based on the assumption that the ion temperature is balanced between the energy exchange term and the frictional heating term with the neutrals. However, the heating by ambient electrons could be a nontrivial heat source where the electron density is high, i.e., on the dayside and the *F* region at high latitudes [*St-Maurice and Hanson*, 1982; *Killeen et al.*, 1984]. In these regions, T_i could deviate from the energy balance assumption as shown in equation (4) due to the ion-electron energy coupling. In other words, T_i was underestimated in the Joule heating rate as a form of the neutral-ion energy coupling. Therefore, the Joule heating rate turned out to be smaller than the complete neutral-ion collisional heating rate in these regions. Furthermore, the difference between the Joule heating rate and the complete neutral-ion collisional heating rate most likely originates from photoelectrons. This is because photoelectron heating is one of the major heat sources for the

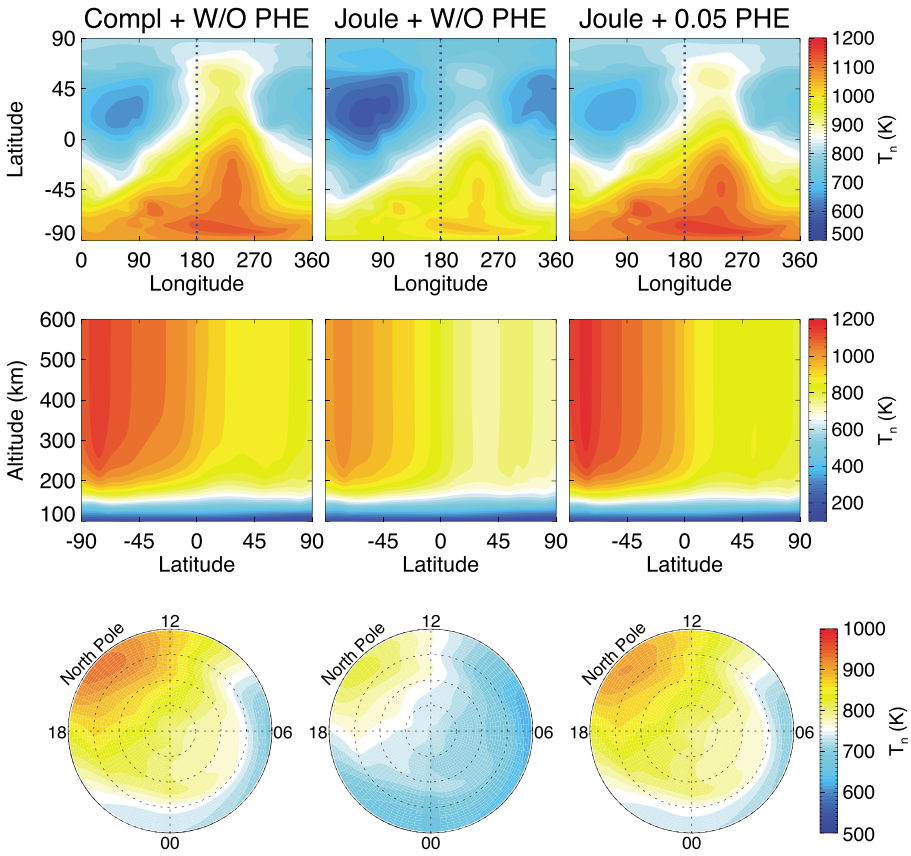

Figure 2. The comparison of T_n between the (left column) Complete simulation, the (middle column) Joule simulation, and the (right column) Joule simulation with 0.05 PHE at 00 UT on 24 December 2012. (top row) The 300 km altitude slice. (middle row) The 180° longitudinal slice. (bottom row) The north polar cap above 50° latitude.

ambient thermal electrons on the dayside [*Nagy and Banks*, 1970; *Rasussen et al.*, 1988; *Smithtro and Solomon*, 2008]. The thermal electrons heated through collisions with photoelectrons subsequently transfer thermal energy to ions, leading to a deviation from the neutral energy balance assumption of T_i. Therefore, the nonzero photoelectron heating efficiency used to calculate T_n applied in the case using the Joule heating rate (i.e., the simplified neutral-ion collisional heating rate), mimicked the indirect heating process from photoelectrons to neutrals (through the ions) as a direct heating process.

Figure 3 shows the percentage difference of the neutral temperature between the Complete simulation and the Joule simulation, as expressed in equation (10), at 00 UT on 24 December (i.e., the end of the last simulation day) at 140 km, 250 km, and 400 km. At 140 km, the difference was within 8%, and the northern polar region had a higher percentage difference than other regions. At 250 km, the difference increased to approximately 12% in the Northern Hemisphere, and about 8% in the Southern Hemisphere. At 400 km, the percentage difference maximized at around 15% in the low-latitude region, which was consistent with *St-Maurice and Hanson* [1982], *Killeen et al.* [1984], and *Schunk and Nagy* [2009], who found that the ion-electron energy coupling played a less important role for the ion temperature at high latitudes than it did at low and middle latitudes because the electron density was generally lower at high latitudes. Specifically, T_n was underestimated by about 10–12% in the polar regions and by about 6% on the nightside in the Joule simulation. It was also found that the percentage difference in T_n was higher around the *F* region (400 km) than around the *E* region (140 km). This could be caused by two reasons: (a) the *E* region electron density was generally lower than the *F* region density, thus the *E* region ion temperature can be better approximated by a balance through energy coupling with the neutrals than the *F* region ion temperature; (b) the neutral atmosphere decreases with altitude, which makes the thermosphere at *E* region altitudes more difficult to heat through neutral-ion collisional heating (or Joule heating) [*Deng et al.*, 2011].

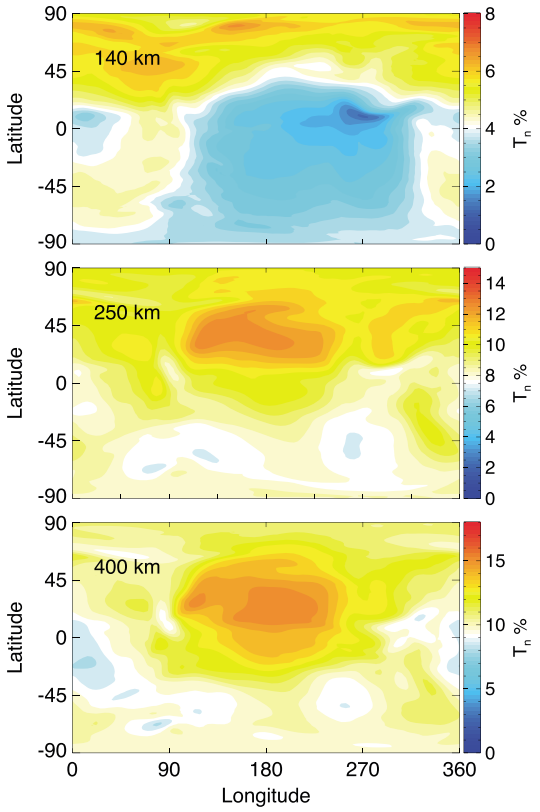

Figure 3. The percentage difference of T_n between the Complete and the Joule simulations, i.e., $T_n\% = \frac{(T_n)_C - (T_n)_J}{(T_n)_C} \times 100\%$, at (top) 140 km, (middle) 250 km, and (bottom) 400 km.

In Figure 4, the colored contours show the difference of the time rate of change of the neutral temperature due to the neutral-ion energy coupling between the Complete and the Joule simulations at 140 km, 250 km, and 400 km. The difference was about 2 orders smaller at 140 km than at 250 km or 400 km, and it was negative around the polar auroral bands at 140 km where the ion temperature was slightly higher than the electron temperature due to the large frictional heating with the neutrals. As shown in equation (17), when T_i becomes higher than T_e, the difference of the heating rate becomes negative, meaning that the Joule heating approximation would cause excess heating in these locations. The vertical profile of the ion-neutral frictional heating will be further discussed below. The model limits the electron temperature so that it can be not less than 90% of the ion temperature for stability purposes. At 250 km, the difference reached a peak around 20°–45° latitude on the dayside and decreased toward both polar regions. At 400 km, the difference maximized around the geographic equator and generally decreased with latitude but was relatively large on the dayside and weak on the nightside. There was also a localized maximum in the auroral zone in the Southern Hemisphere, which could be due to a large deviation of T_i from the energy balance assumption in the auroral band with high electron densities.

Equation (17) shows that the difference between the complete neutral-ion collisional heating and the Joule heating rate is proportional to $\frac{n_i}{T_e^{3/2}}(T_e - T_i)$. This term is contoured by the dotted lines in Figure 4. The contour of this proportional term generally agrees with that of difference in the time rate of change of T_n at 250 km and 400 km, which, once again, indicates that the difference between the complete neutral-ion collisional heating rate and the Joule heating rate resulted from the lack of consideration of the ion-electron energy coupling in the Joule heating rate.

One feature to note about the global distribution of T_n is that the percentage difference of T_n in Figure 3 was greater in the Northern Hemisphere than in the Southern Hemisphere. This was caused by two factors. First, as shown in Figure 2, the Southern Hemisphere was generally warmer than the Northern Hemisphere in December. A greater temperature denominator led to a smaller percentage difference even assuming a similar T_n difference between the two hemispheres. Second, the difference of the time rate of change in the neutral temperature, as shown in Figure 4, was generally greater in the Northern Hemisphere than in the Southern Hemisphere at 250 km, which indicates a greater T_n difference in the Northern Hemisphere.

There were some slight inconsistencies between the colored contour and the line contour at 400 km, which is expected because assumptions have been made in the derivation for equation (17), such as using mean masses for simplification, equality of the mean masses between the ions and neutrals, and assuming constant ion mean mass. Further, neutral density variations were assumed to be negligible. The uncertainty of these assumptions could increase in the *F* region where transport processes become important, and the variations in mass density could become larger.

Figure 5 shows altitudinal profiles of the three major ion thermal sources and losses: the ion-electron heat transfer $Q_T(I-E)$, the ion-neutral frictional heating rate $Q_F(I-N)$, and the negative ion-neutral heat transfer term $-Q_T(I-N)$ as presented in equations (18)–(20) at three different locations. On the dayside, the ion

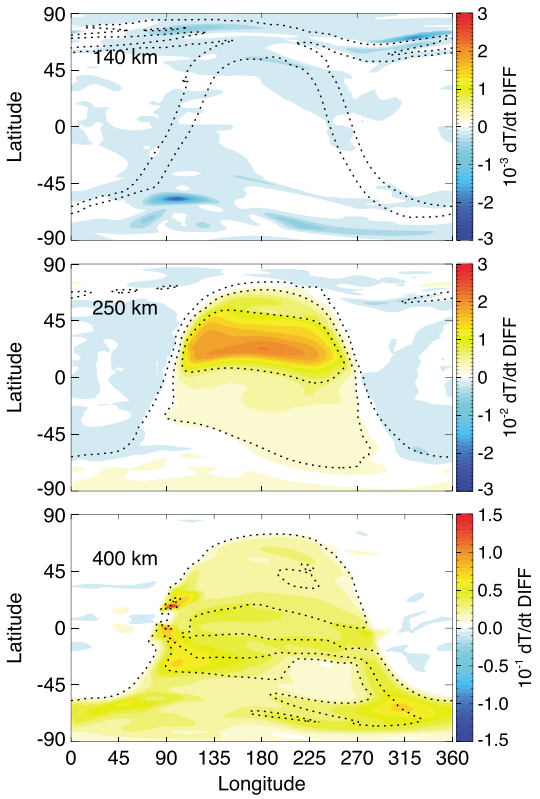

Figure 4. The color contour shows the difference of the time rate of change of T_n due to the neutral-ion energy coupling between the Complete and Joule simulations at (top) 140 km, (middle) 250 km, and (bottom) 400 km. The unit is in $Km^{-3}s^{-1}$. The dotted line contours the term on the right side of equation (17).

temperature was approximately balanced by the ion-neutral energy coupling below 150 km altitude (i.e., energy gained by frictional heating was lost by heat transfer). The ion-electron heat transfer rate increased quickly with altitude, and the ion temperature became a balance between the ion-electron and ion-neutral heat transfer rates around the *F* region. The transition region of the energy balance is at approximately 180 km. This means that the Joule heating rate is a good approximation of the neutral-ion collisional heating rate in the *E* region on the dayside but not in the *F* region. In the polar region, the ion energy balance was primarily between the frictional heating and heat transfer to the neutrals, until the electron heat transfer became a dominant source of energy above around 350 km. This shows that the Joule heating rate is a relatively good approximation in the high-latitude region below 350 km. On the nightside, the ion-electron heat transfer was 1 to 2 orders of magnitude smaller than the other two terms throughout most of the plotted altitudes. Thus, the Joule heating rate was always a good approximate form of the neutral-ion collisional heating rate on the nightside. The frictional heating rate (i.e., yellow line) had a peak in the *E* region. This indicates a large heat source for ions by friction with neutrals in this region, such that T_i could be greater than T_e. This helps to explain the negative ion-electron heating rate around 100 km in the polar region and on the nightside. Note that on the nightside between the *E* region and *F* region, the ion temperature equation is balanced by other terms, such as thermal conduction, instead of only being balanced by friction and heat transfer.

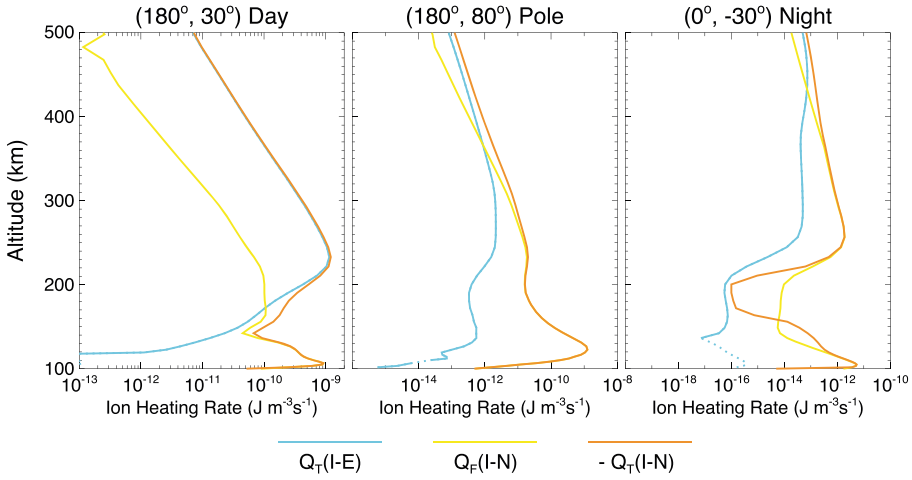

Figure 5. The altitudinal profiles of the ion-electron heat transfer rate (blue), the ion-neutral frictional heating rate (yellow), and the negative ion-neutral heat transfer rate (orange) at three geographic locations at 00 UT of the last day of the simulation.

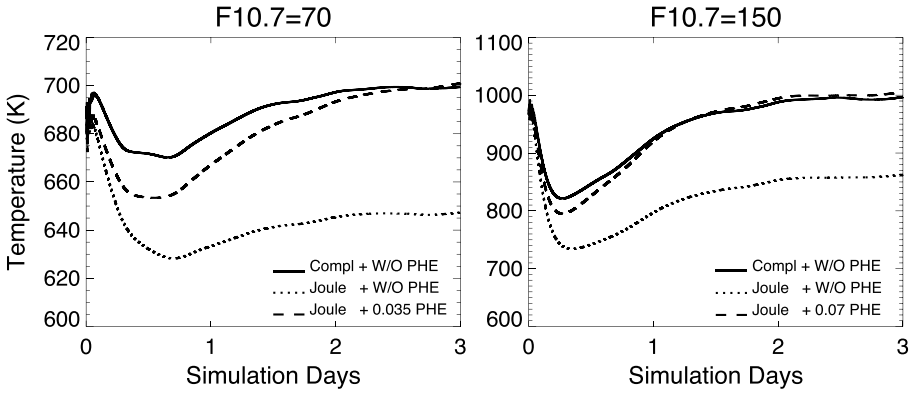

Figure 6. In the same format as Figure 1. The temporal evolution of the global averaged T_n when (left) $F_{10.7} = 70$ sfu and (right) $F_{10.7} = 150$ sfu.

3.2. $F_{10.7}$ Dependence

Considering the underestimation of T_n by the Joule heating rate was mainly caused by the neglect of the indirect heating from electrons to neutrals (through ions) and photoelectron heating was the main way to make up this short fall, it may be expected that the performance of the Joule heating rate (with the 5% PHE) was solar condition dependent. Figure 6 shows the evolution of T_n of the same set of simulations as in Figure 1 but with $F_{10.7} = 70$ sfu (left) and $F_{10.7} = 150$ sfu (right). When the solar activity was low (i.e., $F_{10.7} = 70$ sfu), the global averaged T_n was underestimated by about 50 K (~7%) compared with the Complete simulation in steady state (i.e., at the end of the three simulation days). A photoelectron heating efficiency of 0.035 for the neutral atmosphere compensated for the indirect heating. When the solar radiance was high (i.e., $F_{10.7} = 150$ sfu), the Joule simulation underestimated the global averaged T_n by about 140 K (~14%), which could be compensated by a neutral photoelectron heating efficiency of 0.07. During a medium solar condition with $F_{10.7} = 110$ sfu, as shown in Figure 1, the global averaged T_n in the Joule simulation was approximately 90 K (~11%) cooler than it was in the Complete simulation, which required a photoelectron heating efficiency of 0.05 for compensation. These simulation results suggest a linear relation possibly existing between $F_{10.7}$ and the performance of the Joule heating rate. An increase of 10 sfu of $F_{10.7}$ caused about 1% underestimation of T_n in a simulation using Joule heating rate with no photoelectron heating. The photoelectron heating efficiency increased by 0.015 when $F_{10.7}$ increased from 70 sfu to 110 sfu and increased by 0.02 when $F_{10.7}$ was increased by 40 from 110 sfu to 150 sfu. This indicates that the PHE for the neutral atmosphere that was required for compensating T_n in Joule simulations tended to increase faster with $F_{10.7}$ during high solar conditions, and the electron-ion heat transfer becomes more important nonlinearly as solar activity increases.

4. Discussion and Conclusion

This paper has discussed the performance of the Joule heating rate as an approximate form of the neutral-ion collisional heating rate in the neutral energy equation in the Global Ionosphere-Thermosphere Model. This approximation was valid where the ion-electron collisional heating was negligible and the ion temperature could be approximated by a balance between energy coupling with the neutrals. It has been shown that the global average thermospheric temperature was underestimated by ~11% in the Joule simulation at solar medium (i.e., $F_{10.7}$ equal to 110 sfu) and quiet geomagnetic conditions. The percentage difference of T_n between the two simulations generally decreased from the dayside to the nightside, and from high to low altitudes. At 400 km, the Joule approximation underestimated the neutral temperature by about 15% on the dayside, by about 10–12% in the polar regions, and by about 6% on the nightside. The discrepancy between the Joule heating rate and the Complete neutral-ion collisional heating rate is mainly due to the neglect of the ion-electron heating in the ion energy equation. However, the ion-electron energy coupling can be a nontrivial thermal source for ions in the dayside *F* region and in the higher-altitude polar region.

By increasing the photoelectron heating efficiency of the neutral atmosphere, the underestimation of T_n was compensated for quite adequately. A global ionosphere-thermosphere model that used the Joule heating rate as an approximation of the neutral-ion energy coupling usually applied a PHE for the neutral atmosphere to match model results with observations. However, there has been few studies quantifying the direct heating

from photoelectrons to the neutrals. It was found that there existed a roughly linear relation between the performance of the Joule heating approximation and solar activity. Higher $F_{10.7}$ led to a larger discrepancy in T_n in a simulation using Joule heating rate without the employment of a neutral photoelectron heating efficiency. The compensating neutral PHE increased with solar activity as well. It appeared that the indirect heating of neutrals by electrons increased more efficiently at a high level of solar activity. Beside solar activity, solar wind condition and particle precipitation at high latitude could possibly affect the performance of the Joule heating rate because the convection pattern and auroral activity could effectively change the dynamics of the ionosphere and thermosphere. Further study is needed to investigate the performance of the Joule heating approximation during geomagnetic disturbances. A global IT model should be careful when using the Joule heating rate as an approximate form of the neutral-ion collisional heating rate. Using a fixed neutral PHE to compensate for the loss of the indirect heating from thermal electrons to neutrals may not be proper because the indirect heating from electrons to neutrals can be $F_{10.7}$ dependent. It should also be noted that compensating for one heating source with another may allow quantities such as orbit-averaged mass density to compare quite well with measurement. In addition, since the main area of the temperature difference was on the dayside, and the photoelectron heating also worked on the dayside, any data-model differences caused by issues using the photoelectron heating instead of the complete equation set would be quite subtle during quiet times, as evidence by the comparisons shown here between the two simulations.

Acknowledgments

This work was partially supported by NASA grant NNX09AJ59G and NSF grants AGS1242787 and AGS1138938. We would like to acknowledge high-performance computing support from Yellowstone (ark:/90890) provided by NCAR's Computational and Information Systems Laboratory, sponsored by the National Science Foundation. We would also like to thank NASA's supercomputers, Pleiades (http://www.nas.nasa.gov/hecc/resources/pleiades.html) for conducting the simulations in this study. The GITM simulation data for this case are available upon request from the authors.

References

Aggarwal, K., N. Nath, and C. Setty (1979), Collision frequency and transport properties of electrons in the ionosphere, *Planet. Space Sci.*, *27*(6), 753–768.

Banks, P., J. Foster, and J. Doupnik (1981), Chatanika radar observations relating to the latitudinal and local time variations of Joule heating, *J. Geophys. Res.*, *86*(A8), 6869–6878.

Banks, P. M., and G. Kockarts (1973), *Aeronomy*, Academic Press, New York.

Barth, C., G. Lu, and R. Roble (2009), Joule heating and nitric oxide in the thermosphere, *J. Geophys. Res.*, *114*, A05301, doi:10.1029/2008JA013765.

Brekke, A. (2012), *Physics of the Upper Polar Atmosphere*, Springer, Berlin.

Burrell, A. G., A. Goel, A. J. Ridley, and D. S. Bernstein (2015), Correction of the photoelectron heating efficiency with the global ionosphere-thermosphere model using retrospective cost model refinement, *J. Atmos. Sol. Terr. Phys.*, *124*, 30–38, doi:10.1016/j.jastp.2015.01.004.

Codrescu, M., T. Fuller-Rowell, and J. Foster (1995), On the importance of E-field variability for Joule heating in the high-latitude thermosphere, *Geophys. Res. Lett.*, *22*(17), 2393–2396.

Cole, K. (1971), Electrodynamic heating and movement of the thermosphere, *Planet. Space Sci.*, *19*(1), 59–75.

Cole, K. D. (1962), Joule heating of the upper atmosphere, *Aust. J. Phys.*, *15*, 223, doi:10.1071/PH620223.

Deng, Y., and A. J. Ridley (2007), Possible reasons for underestimating Joule heating in global models: E field variability, spatial resolution, and vertical velocity, *J. Geophys. Res.*, *112*, A09308, doi:10.1029/2006JA012006.

Deng, Y., T. J. Fuller-Rowell, R. A. Akmaev, and A. J. Ridley (2011), Impact of the altitudinal Joule heating distribution on the thermosphere, *J. Geophys. Res.*, *116*, A05313, doi:10.1029/2010JA016019.

Emery, B. A., C. Lathuillere, P. G. Richards, R. G. Roble, M. J. Buonsanto, D. J. Knipp, P. Wilkinson, D. P. Sipler, and R. Niciejewski (1999), Time dependent thermospheric neutral response to the 2–11 November 1993 storm period, *J. Atmos. Sol. Terr. Phys.*, *61*, 329–350, doi:10.1016/S1364-6826(98)00137-0.

Fuller-Rowell, T., M. Codrescu, H. Rishbeth, R. Moffett, and S. Quegan (1996), On the seasonal response of the thermosphere and ionosphere to geomagnetic storms, *J. Geophys. Res.*, *101*(A2), 2343–2353.

Fuller-Rowell, T. J., and D. S. Evans (1987), Height-integrated Pedersen and Hall conductivity patterns inferred from the TIROS-NOAA satellite data, *J. Geophys. Res.*, *92*, 7606–7618, doi:10.1029/JA092iA07p07606.

Fuller-Rowell, T. J., and D. Rees (1980), A three-dimensional time-dependent global model of the thermosphere, *J. Atmos. Sci.*, *37*, 2545–2567, doi:10.1175/1520-0469(1980)037<2545:ATDTDG>2.0.CO;2.

Gary, J., R. Heelis, and J. Thayer (1995), Summary of field-aligned Poynting flux observations from DE 2, *Geophys. Res. Lett.*, *22*(14), 1861–1864.

Hedin, A. E., et al. (1977), A global thermospheric model based on mass spectrometer and incoherent scatter data MSIS, 1. N_2 density and temperature, *J. Geophys. Res.*, *82*(16), 2139–2147, doi:10.1029/JA082i016p02139.

Heelis, R., and W. Coley (1988), Global and local Joule heating effects seen by DE 2, *J. Geophys. Res.*, *93*(A7), 7551–7557.

Killeen, T. L., P. B. Hays, G. R. Carignan, R. H. Heelis, W. B. Hanson, N. W. Spencer, and L. H. Brace (1984), Ion-neutral coupling in the high-latitude f region: Evaluation of ion heating terms from Dynamics Explorer 2, *J. Geophys. Res.*, *89*, 7495–7508, doi:10.1029/JA089iA09p07495.

Liu, H., and H. Lühr (2005), Strong disturbance of the upper thermospheric density due to magnetic storms: Champ observations, *J. Geophys. Res.*, *110*, A09S29, doi:10.1029/2004JA010908.

Maute, A. (2011), *TIEGCM V 1.94 Model Description*, Natl. Cent. for Atmos. Res., Boulder, Colo.

Nagy, A., and P. Banks (1970), Photoelectron fluxes in the ionosphere, *J. Geophys. Res.*, *75*(31), 6260–6270.

Rasussen, C. E., J. J. Sojka, R. W. Schunk, V. B. Wickwar, and O. de la Beaujardiere (1988), Comparison of simultaneous Chatanika and Millstone Hill temperature measurements with ionospheric model predictions, *J. Geophys. Res.*, *93*, 1922–1932, doi:10.1029/JA093iA03p01922.

Richards, P., and D. Torr (1983), A simple theoretical model for calculating and parameterizing the ionospheric photoelectron flux, *J. Geophys. Res.*, *88*(A3), 2155–2162.

Richmond, A. D. (1995), Ionospheric electrodynamics using magnetic apex coordinates, *J. Geomagn. Geoelectr.*, *47*, 191–212.

Ridley, A., Y. Deng, and G. Tòth (2006), The global ionosphere-thermosphere model, *J. Atmos. Sol. Terr. Phys.*, *68*, 839–864, doi:10.1016/j.jastp.2006.01.008.

Roble, R. (1975), The calculated and observed diurnal variation of the ionosphere over Millstone Hill on March 23–24, 1970, *Planet. Space Sci.*, *23*, 1017–1033, doi:10.1016/0032-0633(75)90192-0.
Roble, R., and B. Emery (1983), On the global mean temperature of the thermosphere, *Planet. Space Sci.*, *31*(6), 597–614.
Roble, R. G., E. Ridley, A. Richmond, and R. Dickinson (1988), A coupled thermosphere/ionosphere general circulation model, *Geophys. Res. Lett.*, *15*, 1325–1328, doi:10.1029/GL015i012p01325.
Rodger, A., G. Wells, R. Moffett, and G. Bailey (2001), The variability of Joule heating, and its effects on the ionosphere and thermosphere, *Ann. Geophys.*, *19*, 773–781.
Schunk, R., and A. Nagy (2009), *Ionospheres: Physics, Plasma Physics, and Chemistry*, Cambridge Univ. Press, Cambridge, U. K.
Schunk, R. W. (1975), Transport equations for aeronomy, *Planet. Space Sci.*, *23*, 437–485, doi:10.1016/0032-0633(75)90118-X.
Smithtro, C. G., and S. C. Solomon (2008), An improved parameterization of thermal electron heating by photoelectrons, with application to an x17 flare, *J. Geophys. Res.*, *113*, A08307, doi:10.1029/2008JA013077.
St-Maurice, J.-P., and W. Hanson (1982), Ion frictional heating at high latitudes and its possible use for an in situ determination of neutral thermospheric winds and temperatures, *J. Geophys. Res.*, *87*(A9), 7580–7602.
Strangeway, R. J. (2012), The equivalence of Joule dissipation and frictional heating in the collisional ionosphere, *J. Geophys. Res.*, *117*, A02310, doi:10.1029/2011JA017302.
Swartz, W. E., and J. S. Nisbet (1972), Revised calculations of *F* region ambient electron heating by photoelectrons, *J. Geophys. Res.*, *77*, 6259–6261, doi:10.1029/JA077i031p06259.
Thayer, J. (1998), Height-resolved Joule heating rates in the high-latitude *E* region and the influence of neutral winds, *J. Geophys. Res.*, *103*(A1), 471–487.
Thayer, J. P., and J. Semeter (2004), The convergence of magnetospheric energy flux in the polar atmosphere, *J. Atmos. Sol. Terr. Phys.*, *66*, 807–824, doi:10.1016/j.jastp.2004.01.035.
Torr, M., D. Torr, and P. Richards (1980), The solar ultraviolet heating efficiency of the midlatitude thermosphere, *Geophys. Res. Lett.*, *7*(5), 373–376.
Torr, M. R., D. Torr, P. Richards, and S. Yung (1990), Mid-and low-latitude model of thermospheric emissions: 1. O^+ (^2P) 7320 Å and N2 ($2P$) 3371 Å, *J. Geophys. Res.*, *95*(A12), 21,147–21,168.
Vichare, G., A. J. Ridley, and E. Yigğit (2012), Quiet-time low latitude ionospheric electrodynamics in the non-hydrostatic global ionosphere-thermosphere model, *J. Atmos. Sol. Terr. Phys.*, *80*, 161–172, doi:10.1016/j.jastp.2012.01.009.
Weimer, D. R. (2005), Improved ionospheric electrodynamic models and application to calculating Joule heating rates, *J. Geophys. Res.*, *110*, A05306, doi:10.1029/2004JA010884.
Zhu, X., E. R. Talaat, J. B. H. Baker, and J.-H. Yee (2005), A self-consistent derivation of ion drag and Joule heating for atmospheric dynamics in the thermosphere, *Ann. Geophys.*, *23*, 3313–3322, doi:10.5194/angeo-23-3313-2005.